Quantification of road vehicle handling quality using a compensatory steering controller

Giovanni Braghieri
Research Student

Alexander Haslam
Masters Student
(now at McLaren Racing)

Michalis Sideris
Masters Student
(now at McLaren Racing)

Julian Timings
Research Student

David Cole *
Senior Lecturer
Department of Engineering
University of Cambridge
Cambridge
CB2 1PZ, UK
Email: djc13@cam.ac.uk

Criteria for stability and controllability of road vehicles are briefly reviewed and it is argued that there is a need for criteria that might better relate to subjective ratings by drivers. The variance of a driver's closed-loop control action against random disturbances acting on the vehicle is proposed as a realistic criterion that might relate to a driver's assessment of the vehicle. A nonlinear vehicle model with five degrees of freedom, negotiating a ninety-degree bend in minimum time is the basis for the theoretical study. The vehicle model is run with the centre of mass in two different positions. It is found that the variance of the driver's compensatory steering control varies significantly through the manoeuvre, reaching a peak at about mid-corner. The corresponding variance in the lateral path error of the vehicle also peaks at about the same position in the manoeuvre. Comparison of these variances to existing stability and controllability criteria shows that the variance of the compensatory control might reveal aspects of the handling behaviour that the existing criteria do not. Recommendations for further work are given, and include a program of driving simulator experiments or track tests to correlate the new criteria against subjective ratings by human drivers.

1 Introduction

Automotive engineers tasked with tuning the handling behaviour of a vehicle often use quantitative objective criteria to assess stability and controllability under various operating conditions. An ideal criterion would be predictable from the design parameters of the vehicle and correlate well with subjective assessments. Many criteria have been used in the past. The use of *stability and controllability derivatives* originally employed in the aircraft industry is advocated in [1]. If the total lateral force and yaw moment applied to the vehicle by the tyres are denoted by F_t and M_t then in the case of the linear operating regime they can be expressed in terms of the vehicle sideslip angle β, yaw rate $\dot{\psi}$, front road wheel steer angle δ and six partial derivatives:

$$F_t = (\frac{\partial F_t}{\partial \beta})\beta + (\frac{\partial F_t}{\partial \dot{\psi}})\dot{\psi} + (\frac{\partial F_t}{\partial \delta})\delta \quad (1)$$

$$M_t = (\frac{\partial M_t}{\partial \beta})\beta + (\frac{\partial M_t}{\partial \dot{\psi}})\dot{\psi} + (\frac{\partial M_t}{\partial \delta})\delta \quad (2)$$

Numerical values of the six partial derivatives can give insight to the handling behaviour of the vehicle. The analysis can be extended to the case of nonlinear vehicles operating near the limit of adhesion [1].

A *handling diagram* is constructed in [2] to depict some aspects of the handling behaviour of a vehicle. Normalized characteristics of lateral force against slip angle for front and rear axles are used to construct the diagram. Equilibrium points and their stability can be determined for combinations of vehicle speed and steering angle. More information about the transient behaviour of a vehicle can be obtained by plotting a *phase portrait* [3, 4]. The portrait depicts the trajectories of two states of the vehicle, for example yaw rate and lateral velocity. Equilibrium points and their stability can be

*Address all correspondence to this author.

determined by observing convergence or divergence of the trajectories. A limitation of the phase portrait is that only a limited range of operating conditions can be depicted on an individual portrait.

Frozen-time eigenvalues for time varying systems are investigated in [5, 6]. Conditions for which a slowly time varying system is asymptotically stable if the frozen system is stable are derived. An eigenvalue analysis of a linearized, time-varying state space model of a motorcycle was undertaken in [7]. Root loci of the poles of the motorcycle system were plotted as they varied with time through various manoeuvres. These frozen-time eigenvalues predicted the motorcycle's stability accurately, judged against a nonlinear simulation. It was stressed however that the method should be used with utmost care when inferring stability, especially when eigenvalues cross the imaginary axis.

The concept of *practical stability* was applied to a motorcycle in [8]. A transient disturbance was applied to a nonlinear motorcycle model at the beginning of a manoeuvre and then the subsequent growth or decay of oscillations during the course of the manoeuvre was used to assess the stability. This approach was further developed in [9] by adopting ideas from tube-based robust model predictive control. Instead of a transient disturbance, a continual random disturbance was applied to a simulated nonlinear vehicle negotiating a lap of a circuit. A simulated driver was assumed to perform closed-loop feedback control to compensate for the effect of the random disturbance and keep the vehicle close to the optimal path. The trade-off between the variance of the compensatory steering control (a measure of the driver's physical workload) and the lap time was quantified. A disadavantage of the method was that the variance of compensatory steering control was determined from an ensemble 1000 time domain simulations, which was computationally expensive.

The work described in the present paper extends the approach in [9] by calculating the variance of the simulated driver's compensatory control responses directly, rather than by simulating an ensemble of time domain responses. In addition, the way in which the variance of the compensatory responses changes through the manoeuvre is examined, and compared against several existing stability and controllability criteria. It is anticipated that the variance of the driver's compensatory control action and the variance of the vehicle's lateral path dispalcement from the nominal path might relate to the driver's subjective assessment of the stability and controllability of the vehicle. In addition, by examining the way in which the variances change through the manoeuvre, it might be possible to tune the vehicle to behave in a desirable manner at various stages of the manoeuvre. The proposed new criteria differ from existing criteria by accounting for the closed-loop dynamics of the driver and vehicle, rather than considering only the open-loop dynamics of the vehicle without consideration of the driver.

Section 2 describes the nonlinear vehicle model and Section 3 summarises the algorithm used to calculate the nominal

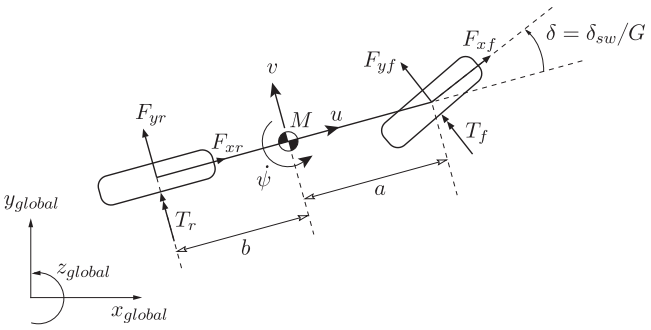

Fig. 1: Vehicle model with associated forces and dimensions.

driver controls (driver/brake torque and steering angle) to negotiate a ninety-degree bend in minimum time. The compensatory steering controller is presented in Section 4, and the method for calculating the variance of its response is set out in Section 5. Results of the variance calculation for two different vehicles are presented in Section 6 and comparisons to existing stability and controllability criteria are discussed in Section 7. Aspects of the work were documented in [10, 11].

2 Vehicle model

The vehicle model is similar to that employed in [9]. The lateral and yaw dynamics of the vehicle are represented by the familiar single-track 'bicycle' model with five degrees of freedom as shown in Fig. 1. The model complexity is appropriate for demonstrating the new stability and controllability criteria, but a more detailed model would likely be required to investigate the performance of a specific vehicle. The forces generated by left and right tyres on an axle are combined and throughout this paper all parameter values associated with the tyres relate to the combined left and right tires on the axle. The equations of motion are:

$$M(\dot{v}+u\dot{\psi}) = F_{yf}\cos\delta + F_{xf}\sin\delta + F_{yr} + F_y \quad (3a)$$

$$I_z\ddot{\psi} = a(F_{yf}\cos\delta + F_{xf}\sin\delta) - bF_{yr} + M_z \quad (3b)$$

$$M(\dot{u}-v\dot{\psi}) = F_{xf}\cos\delta - F_{yf}\sin\delta + F_{xr} \quad (3c)$$

$$I_f\ddot{\theta}_f = T_f - F_{xf}r_f \quad (3d)$$

$$I_r\ddot{\theta}_r = T_r - F_{xr}r_r \quad (3e)$$

The parameters and their nominal values are defined in Table 1. δ is the front road wheel steer angle, $T_{f,r}$ the axle torques and $\theta_{f,r}$ the wheel/axle angular displacements. The subscripts f,r indicate front and rear and x,y indicate longitudinal and lateral. A lateral force F_y and a yaw moment M_z applied at the centre of mass of the vehicle act as disturbances, such as might arise from road roughness, friction variations or wind gusts. A single control torque T represents a combined drive action (if $T > 0$) and brake action (if $T < 0$). Assuming the vehicle is rear wheel drive, the torque

T is distributed to the front and rear wheels such that

$$T_f = b_f(1-H(T))T \tag{4}$$
$$T_r = T - T_f \tag{5}$$

where $H(\cdot)$ is the Heaviside step function and b_f is the brake balance (fraction of braking torque applied to the front axle).

The tyre forces are expressed as functions of the lateral and longitudinal slips. The slips are defined as:

$$\alpha_f = \delta - \frac{v+\dot{\psi}a}{|u|}, \quad \alpha_r = -\frac{v-\dot{\psi}b}{|u|} \tag{6}$$
$$\kappa_f = \frac{\dot{\theta}_f r_f - u}{|u|}, \quad \kappa_r = \frac{\dot{\theta}_r r_r - u}{|u|} \tag{7}$$

where α_j is the lateral tyre slip, κ_j is the longitudinal tyre slip and j is f or r. A normalised slip vector is defined [12]:

$$\mathbf{s}_j = \begin{bmatrix} s_{xj} \\ s_{yj} \end{bmatrix} = \frac{C_{\alpha j}}{F_{pj}} \begin{bmatrix} \kappa_j \\ \tan\alpha_j \end{bmatrix} \tag{8}$$

where s is the normalised tyre slip and $C_{\alpha j}$ is the normalised tyre cornering coefficient. The friction circle limits F_{pj} are functions of the static axle loads F_{zj} and of the form:

$$F_{pj} = \frac{F_{zj}}{1+(\frac{2F_{zj}}{3Mg})^3} \tag{9}$$

where F_{zj} is the vertical force on the axle. For the purpose of the present study the height of the vehicle's centre of mass is set to zero, to minimise the number of parameters in the vehicle model and make the results as generic as possible. Thus only static vertical forces are considered so:

$$F_{zf} = \frac{b}{a+b}Mg, \quad F_{zr} = \frac{a}{a+b}Mg \tag{10}$$

The slip coefficient $C_{\alpha j}$ is defined as:

$$C_{\alpha j} = c_1\left(1-\exp\left(-\frac{F_{zj}}{c_2}\right)\right) \tag{11}$$

where c_1 and c_2 are tyre coefficients. Tyre forces can finally be expressed as:

$$\begin{bmatrix} F_{xj} \\ F_{yj} \end{bmatrix} = P(|\mathbf{s}_j|)\frac{F_{pj}}{|\mathbf{s}_j|}\begin{bmatrix} s_{xj} \\ s_{yj} \end{bmatrix} \tag{12}$$

Parameter	Symbol	Value
Mass	M	1050 kg
Moment of inertia about z axis	I_z	1500 kgm^2
Front axle to CoM distance	a	0.92 m
Rear axle to CoM distance	b	1.38 m
Wheel radius	r_f, r_r	0.28 m
Wheel/axle moment of inertia	I_f, I_r	2 kgm^2
Front brake balance	b_f	0.6
NMS natural frequency	ω_n	18.85 rad/s
NMS damping factor	ξ_n	0.707
Steering gear ratio	G	17
Magic formula coefficient	B	1.03
Magic formula coefficient	C	1.60
Magic formula coefficient	D	1.36
Magic formula coefficient	E	0.00
Tyre coefficient	c_1	69 kN/rad
Tyre coefficient	c_2	1.4 kN
Gravitational constant	g	9.81 m/s^2
Discrete time step	T_d	0.02 s

Table 1: Vehicle model parameters and nominal values. Tyre parameter values are per axle.

where the function $P(s)$ is Pacejka's magic formula [2]:

$$P(s) = D\sin(C\arctan(Bs - E(Bs - \arctan(Bs)))) \tag{13}$$

The values of these coefficients, as well as c_1 and c_2, are shown in Table 1, and are identical for the front and rear axles. Lateral front tyre forces for a range of longitudinal slips are shown in Fig. 2.

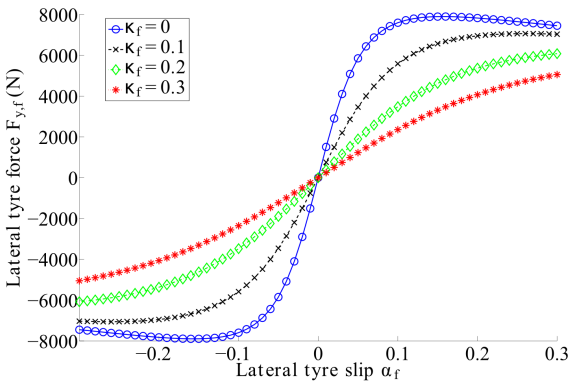

Fig. 2: Lateral tyre force for one axle. The curves show four different levels of longitudinal slip κ. The vertical axle force F_{zj} is 6000 N.

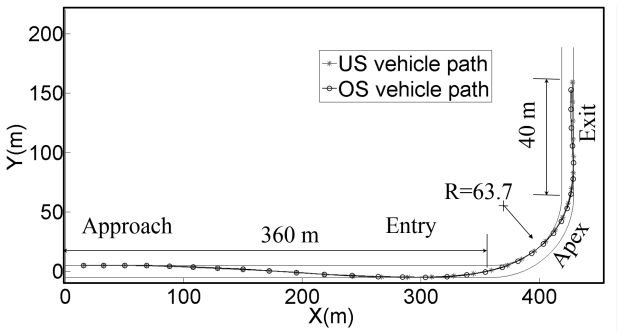

Fig. 3: The road boundaries and the optimal paths of the US and OS vehicles.

The bandwidth-limiting effect of the driver's neuromuscular system (NMS) is represented by a second order low-pass filter acting on the hand wheel angle input δ_{sw} to the vehicle [13, 14], given by:

$$\ddot{\delta}_{sw} + 2\xi_n\omega_n\dot{\delta}_{sw} + \omega_n^2\delta_{sw} = \omega_n^2\delta_{com} \tag{14}$$

where δ_{com} is the commanded hand wheel angle, ξ_n and ω_n are the damping ratio and natural frequency of the NMS; values for these parameters were informed by [15]. The road wheel steering angle is given by

$$\delta = \frac{\delta_{sw}}{G} \tag{15}$$

The nonlinear vehicle dynamics equations can be expressed as

$$\dot{\mathbf{x}} = f(\mathbf{x},\mathbf{u}) \tag{16}$$
$$\mathbf{z} = g(\mathbf{x}) \tag{17}$$

with state vector

$$\mathbf{x} = [v \;\; \dot{\psi} \;\; \psi \;\; u \;\; \dot{\theta}_f \;\; \dot{\theta}_r \;\; \dot{\delta}_{sw} \;\; \delta_{sw}]^T \tag{18}$$

and control input

$$\mathbf{u} = [\delta_{com} \;\; T]^T \tag{19}$$

A linearised representation of (16) and (17) is achieved by performing a linearisation about an arbitrary, possibly non equilibrium point $(\mathbf{x}_0, \mathbf{u}_0)$ to give

$$\dot{\mathbf{x}}_c = \mathbf{A}_c\mathbf{x}_c + \mathbf{B}_c\mathbf{u}_c + \mathbf{F}_c \tag{20}$$
$$\mathbf{z}_c = \mathbf{C}_c\mathbf{x}_\mathbf{c} + \mathbf{G}_c \tag{21}$$

where $\mathbf{x}$ is the state vector and the matrices relate to the Jacobians through

$$\mathbf{A}_c = \left.\frac{\partial f(\mathbf{x},\mathbf{u})}{\partial \mathbf{x}}\right|_{\mathbf{x}_0,\mathbf{u}_0}, \quad \mathbf{B}_c = \left.\frac{\partial f(\mathbf{x},\mathbf{u})}{\partial \mathbf{u}}\right|_{\mathbf{x}_0,\mathbf{u}_0} \tag{22}$$
$$\mathbf{F}_c = f(\mathbf{x}_0,\mathbf{u}_0) - \mathbf{A}_c\mathbf{x}_0 - \mathbf{B}_c\mathbf{u}_0 \tag{23}$$
$$\mathbf{C}_c = \left.\frac{\partial g(\mathbf{x})}{\partial \mathbf{x}}\right|_{\mathbf{x}_0}, \quad \mathbf{G}_c = g(\mathbf{x}_0) - \mathbf{C}_c\mathbf{x}_0 \tag{24}$$

For more details of the linearisation see [9, 16]. Following common practice in the field of Model Predictive Control the system is then discretised. Zero order hold discretisation is used; the subscript k indicates that the object is in discrete time and evaluated at time $t = T_d k$, where T_d is the discrete time step and k is an integer. The system of equations takes the form

$$\mathbf{x}_{k+1} = \mathbf{A}_k\mathbf{x}_k + \mathbf{B}_k\mathbf{u}_k + \mathbf{F}_k \tag{25}$$
$$\mathbf{z}_k = \mathbf{C}_k\mathbf{x}_k + \mathbf{G}_k \tag{26}$$

3 Minimum manoeuvre time calculation

A single 90° bend shown in Fig. 3 is considered. The track is 10 m wide; it starts with a straight section of 360 m, followed by a 90° bend of length 100 m whose centreline has a constant radius of 63.7 m. A long straight section follows, with the simulation terminating 40 m into this. Following [16] the minimum manoeuvre time for the undisturbed vehicle described by (25) and (26) is obtained by formulating a convex optimisation problem that maximises the distance travelled along the centreline in a given time. Optimal controls δ_{sw} and T are calculated for two vehicle configurations. One is defined by the nominal parameter values in Table 1 and has a

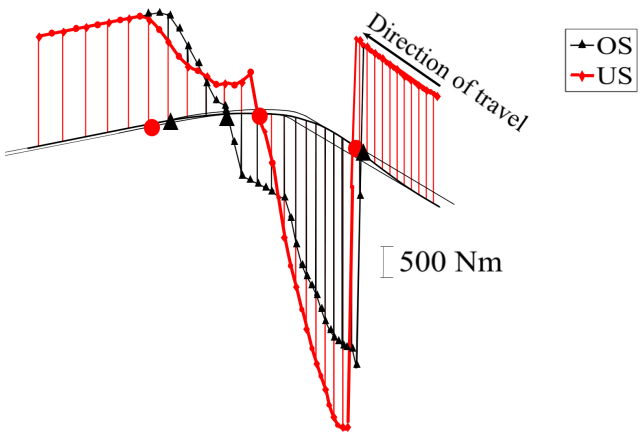

Fig. 4: Optimal torque (T) through the manoeuvre for the US and OS vehicles. The torque is positive (accelerating) if the line is above road level and negative (braking) when the line is below road level. Both vehicles accelerate in the first part of the manoeuvre, then brake at corner entry and accelerate at the exit. The vertical lines correspond to data at time intervals of 0.4 s. The triangles and circles plotted at road level correspond to the three phases of the manoeuvre: braking on entry; transition from braking to accelerating at mid corner; and maximum drive torque at exit.

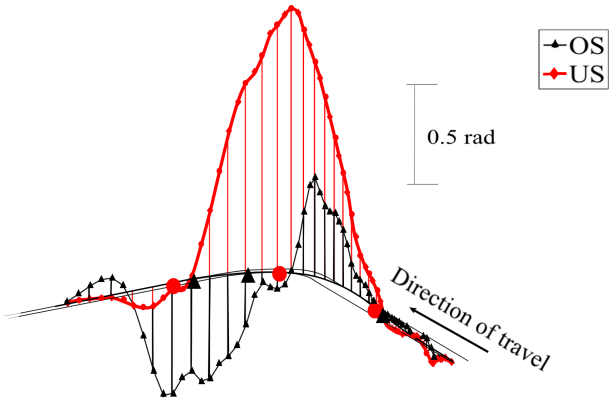

Fig. 5: Optimal hand wheel angle (δ_{sw}) through the manoeuvre for the US and OS vehicles. The steering angle for the US vehicle is positive through most of the corner while it is positive at the beginning of the corner for the OS vehicle and negative (countersteering) towards the exit.

steady-state under-steering (US) characteristic. The other is defined by the same parameter values except for $a = 1.38$ m and $b = 0.92$ m and has an over-steering characteristic (OS) due to the rearward position of the centre of mass (CoM). The brake balance b_f is the same for both vehicles. The vehicle begins on the left-hand boundary at the start of the first straight with speed 30 m/s. The optimisation involves some constraints: the vehicle is required to remain with the road boundaries; the maximum drive torque is 2 kNm; the maximum allowable tire slip at any time is that which gives 0.99 of the maximum feasible horizontal tyre force at that time.

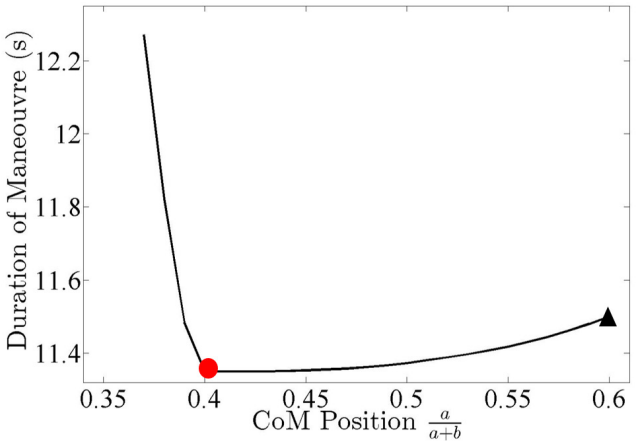

Fig. 6: Relationship between manoeuvre time and centre of mass position. The optimal value to minimise manoeuvre time is 0.42.

Fig. 4 shows the optimal torque control for the US and OS vehicles. The vertical lines correspond to data at time intervals of 0.4 s. The constraint on drive torque means that the torques are equal whilst accelerating on approach to the corner. However the braking point for the US vehicle is a little later than for the OS vehicle and the total braking torque is greater, due to the front-biased brake balance and forward CoM position of the US vehicle. After the apex of the corner the US vehicle begins accelerating earlier than the OS vehicle, but the OS vehicle applies maximum drive torque earlier than the US vehicle. The triangles and circles plotted at road level correspond to these three phases of the manoeuvre: braking on entry; transition from braking to accelerating at mid corner; and maximum drive torque at exit. Fig. 5 shows the optimal hand wheel angle for the US and OS vehicles. Larger angles are required for the US vehicle compared to the OS vehicle. Another notable difference is that a significant countersteering action (negative angle) is applied to the OS vehicle after the apex of the corner. Comparing the torque and steering controls it can be observed that for both vehicles on entry to the bend the steering begins at about the same time as the switch from accleration to braking. After this point the braking torque tends to reduce from its peak value as the steering angle increases. This ensures that the constraint on combined longitudinal and lateral slip is satisfied. For the US vehicle the peak steering angle occurs at about the same time that braking torque reaches zero, which is consistent with the slip at the front axle being limiting. Maximum drive torque is applied to the US vehicle at the point where the steering angle returns to near zero. The coordination of the steering and torque controls of the OS vehicle is different to the US vehicle and consistent with the slip at the rear axle being limiting. The countersteering action begins just before the switch from braking to acceleration and continues for a short while after maximum drive torque is reached.

The effect of CoM position, defined as $a/(a+b)$, on time to complete the manoeuvre is shown in Fig. 6. The brake

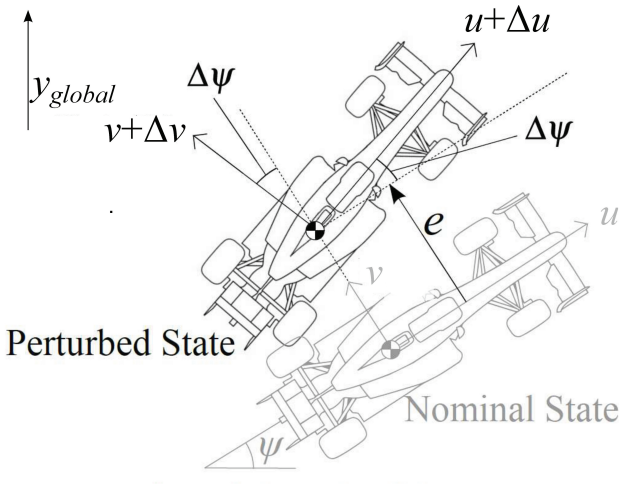

Fig. 7: Vehicle in the nominal and perturbed state. The lateral path error e is shown together with nominal and perturbed longitudinal velocity u, lateral velocity v, and yaw angle ψ.

balance is fixed to the value given in Table 1. Minimum time occurs at $a/(a+b) = 0.42$, which is close to the value of 0.4 specified for the US vehicle.

4 Compensatory controller

In the preceding section the optimal controls to achieve minimum manoeuvre time are calculated. These controls could in principle be applied in a feedforward, open-loop fashion to the vehicle, and in the absence of disturbances and other uncertainties, the nominal trajectory would be achieved. In practice the driver will be required to perform an additional feedback, closed-loop control in order to compensate for disturbances and other uncertainties, and to stabilise the vehicle if necessary. It is the proposition of this paper that the driver's compensatory control action and corresponding vehicle response provide a practical and objective way of quantifying the handling quality of the vehicle as it travels through the manoeuvre.

It will be assumed that the primary function of the driver's compensatory control is to minimise lateral deviation of the vehicle from the nominal optimum trajectory calculated in Section 3. This is an appropriate assumption for a racing driver, but drivers in other situations may have different objectives. The state space equation (20) is augmented to include the lateral displacement as a ninth state.

Referring to Fig. 7 the perturbed longitudinal and lateral velocities are $u+\Delta u$ and $v+\Delta v$ and the perturbed yaw angle is $\psi+\Delta\psi$, so that the time derivative of the lateral path error, neglecting second order terms, can be expressed as:

$$\begin{aligned}\dot{e} &= (v+\Delta v)+(u+\Delta u)\Delta\psi - v \\ &= \Delta v + u\Delta\psi\end{aligned} \tag{27}$$

where $\Delta\psi$ is assumed small. In order to include this expression in the state space equation an additional state is considered:

$$\dot{y} = v + u\psi \tag{28}$$

This equation is not valid for the large angles ψ that might arise in the nominal case. However, when small perturbations are considered about a linearisation point y_0, (28) reduces to

$$\begin{aligned}\dot{y}_0 + \Delta\dot{y} &= (v_0+\Delta v)+(u_0+\Delta u)(\psi_0+\Delta\psi) \\ &= (v_0+u_0\psi_0)+(\Delta v + u_0\Delta\psi + \psi_0\Delta u) \\ \Leftrightarrow \Delta\dot{y} &= \Delta v + u_0\Delta\psi + \psi_0\Delta u\end{aligned} \tag{29}$$

If Δy is to be equivalent to e then it is clear that the linearisation point must be taken about u_0, the current nominal longitudinal velocity. However the linearisation must also be about $\psi_0 = 0$ rather than the true current yaw angle, to ensure that the lateral path error is independent of the nominal heading angle in the global reference frame.

Disturbances $\mathbf{w}$ are considered to cause small perturbations $\Delta\mathbf{x}_k$ about the current nominal state $\bar{\mathbf{x}}_k$, with nominal control input $\bar{\mathbf{u}}_k$. The state space equation can be expressed as

$$\begin{aligned}\mathbf{x}_{k+1} = \bar{\mathbf{x}}_{k+1} + \Delta\mathbf{x}_{k+1} = \mathbf{A}_k(\bar{\mathbf{x}}_k + \\ \Delta\mathbf{x}_k) + \mathbf{B}_k(\bar{\mathbf{u}}_k + \Delta\mathbf{u}_k) + \mathbf{H}_k\mathbf{w}_k + \mathbf{F}_k\end{aligned} \tag{30}$$

where $\mathbf{w}_k$ are the disturbances and $\Delta\mathbf{u}_k$ is the compensatory control action added to the nominal control action.

Disturbances are considered to arise from random lateral force and yaw moment acting at the centre of mass, and random additional handwheel angle arising from neuromuscular noise. It is assumed that all three disturbances are zero mean, Gaussian and uncorrelated. The disturbance covariance matrix takes the following form

$$\mathrm{cov}(w_k) = \begin{bmatrix} \sigma^2_{\delta_{\mathrm{sw,dist}}} & 0 & 0 \\ 0 & \sigma^2_{\mathrm{F_{y,dist}}} & 0 \\ 0 & 0 & \sigma^2_{\mathrm{M_{z,dist}}} \end{bmatrix} \tag{31}$$

where σ denotes standard deviation and the subscripts denote the signal to which the standard deviation relates. Values for the variances of the random force and moment are derived from [17] and are $\sigma_{\mathrm{F_{y,dist}}}$ =730 N and $\sigma_{\mathrm{M_{z,dist}}}$ =360 Nm. Variance of the handwheel angle disturbance is derived from driving simulator experiments [13, 18] and is $\sigma_{\delta_{\mathrm{sw,dist}}}$ =0.1 rad.

The state-space equation (25) can be decomposed as the

nominal disturbance-free dynamics:

$$\bar{\mathbf{x}}_{k+1} = \mathbf{A}_k\bar{\mathbf{x}}_k + \mathbf{B}_k\bar{\mathbf{u}}_k + \mathbf{F}_k \tag{32}$$

and the perturbation dynamics:

$$\Delta\mathbf{x}_{k+1} = \mathbf{A}_k\Delta\mathbf{x}_k + \mathbf{B}_k\Delta\mathbf{u}_k + \mathbf{H}_k\mathbf{w}_k \tag{33}$$

The human driver's compensatory control action is modelled as a Linear Quadratic Regulator (LQR) with full state feedback. Other control theories can be used to represent human control action, such as model predictive control and fuzzy control. An LQR model has been shown to represent measured steering behaviour well [13, 18], and has been shown in some circumstances to be equivalent to model predictive control [14]. Future work will account for sensory and cognitive limitations [19,20]. The objective of the compensatory controller is to provide a control action

$$\Delta\mathbf{u}_k = -\mathbf{K}_k\Delta\mathbf{x}_k \tag{34}$$

that minimises a quadratic cost function [21] comprising a weighted sum of mean square compensatory control action and mean square deviation from the nominal state:

$$J = \sum_{k=1}^{\infty}(\mathbf{x}_k^T\mathbf{Q}\mathbf{x}_k + \mathbf{u}_k^T\mathbf{R}\mathbf{u}_k) \tag{35}$$

where $\mathbf{Q}$ is the state cost matrix and $\mathbf{R}$ the input cost matrix. The two weighting matrices, $\mathbf{Q} = \text{diag}(q_i)$, where $i = 1:9$ and $\mathbf{R} = \text{diag}(r_l)$ where $l = 1:2$, are chosen to achieve an acceptable performance trade-off. To penalise steering action $\Delta\delta_{sw}$ is weighted with $q_7 = 1$ (rad/s)$^{-2}$ and $\Delta\delta_{sw}$ is weighted with $q_8 = 1$ rad^{-2}. Lateral path deviation Δe is weighted with $q_9 = 10$ m^{-2} and heading error $\Delta\psi$ with $q_3 = 1$ rad^{-2}. To discourage significant compensatory braking or acceleration control the weight on ΔT was set to $r_2 = 0.01$ (Nm)$^{-2}$. All other states and controls were weighted with 10^{-6}. If measured driving response data are available it is possible to identify values of the cost function weights [13, 18].

5 Compensatory response calculation

Consider the covariance of (25):

$$\text{cov}(\mathbf{x}_{k+1}) = \text{cov}(\mathbf{A}_k\mathbf{x}_k + \mathbf{B}_k\mathbf{u}_k + \mathbf{H}_k\mathbf{w}_k + \mathbf{F}_k) \tag{36}$$

$\mathbf{x}_k$ can again be further split up into a nominal component $\bar{\mathbf{x}}_k$ with cov($\bar{\mathbf{x}}_k$)=0, and a perturbation $\Delta\mathbf{x}_k$ about this with

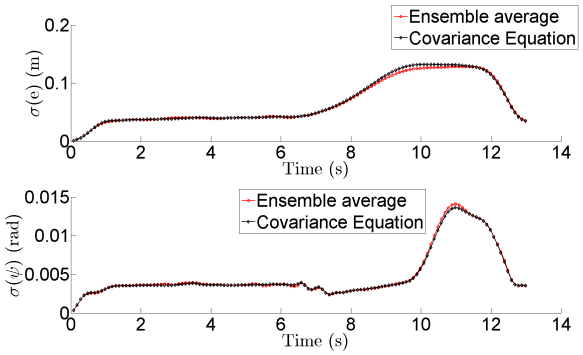

Fig. 8: Standard deviation of the lateral path deviation and heading angle for the US vehicle, calculated using (40) and an ensemble of 1000 time domain responses.

E($\Delta\mathbf{x}_k$)=0. Similarly for $\mathbf{u}_k$ using (33) to give

$$\text{cov}(\mathbf{x}_{k+1}) = \text{cov}(\bar{\mathbf{x}}_{k+1} + \Delta\mathbf{x}_{k+1}) = \text{cov}(\mathbf{A}_k (\bar{\mathbf{x}}_k + \Delta\mathbf{x}_k) + \mathbf{B}_k(\bar{\mathbf{u}}_k + \Delta\mathbf{u}_k) + \mathbf{H}_k\mathbf{w}_k + \mathbf{F}_k) \tag{37}$$

The covariance of the nominal components is zero by definition. The variance of the constant is also zero, so (37) becomes

$$\text{cov}(\mathbf{x}_{k+1}) = \text{cov}(\Delta\mathbf{x}_{k+1}) = \text{cov}(\mathbf{A}_k\Delta\mathbf{x}_k + \mathbf{B}_k\Delta\mathbf{u}_k + \mathbf{H}_k\mathbf{w}_k) \tag{38}$$

The expression for $\Delta\mathbf{u}_k$ (34) can be substituted into (38). Noting that $\mathbf{w}_k$ is uncorrelated with the current vehicle state perturbation [22], the covariance equation becomes

$$\text{cov}(\mathbf{x}_{k+1}) = \text{cov}((\mathbf{A}_k - \mathbf{B}_k\mathbf{K}_k)\Delta\mathbf{x}_k) + \text{cov}(\mathbf{H}_k\mathbf{w}_k) \tag{39}$$

Exploiting the identity cov($\mathbf{Ab}$) = $\mathbf{A}$cov($\mathbf{b}$)$\mathbf{A}^T$, and remembering that cov($\mathbf{x}_k$) = cov($\Delta\mathbf{x}_k$), the covariance equation can finally be expressed as

$$\text{cov}(\mathbf{x}_{k+1}) = (\mathbf{A}_k - \mathbf{B}_k\mathbf{K}_k)\text{cov}(\mathbf{x}_k)(\mathbf{A}_k - \mathbf{B}_k\mathbf{K}_k)^T + \mathbf{H}_k\text{cov}(\mathbf{w}_k)\mathbf{H}_k^T \tag{40}$$

The variances predicted using (40) are compared with those determined numerically from an ensemble of 1000 time domain responses calculated using (33). Fig. 8 shows the time-varying standard deviations of the heading angle and lateral path deviations of the US vehicle calculated using the two methods. It is clear that the analytical and numerical results are consistent with each other.

In order to assess the controllability of the vehicle, the covariance calculation is extended to the control signals. The

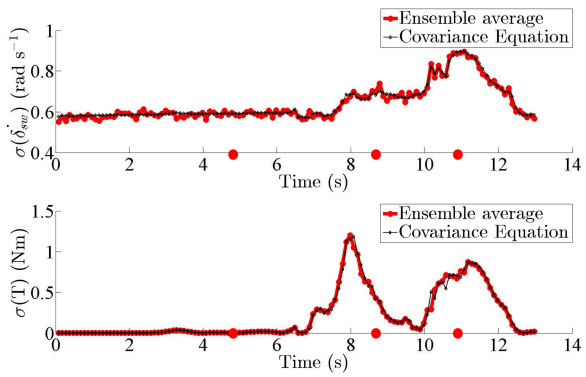

Fig. 9: Standard deviation of the compensatory hand wheel rate calculated using (40) and drive/brake torque for the US vehicle calculated using (42) and an ensemble of 1000 time domain responses.

initial quantities of interest are the hand wheel rate and the drive/brake torque. The hand wheel rate is chosen over the hand wheel angle because it has been argued that the physical difficulty arises more from changing the angle than holding the angle constant [23]. This quantity can be calculated from (40) since $\dot{\delta}_{sw}$ is one of the vehicle states. However, this is not the case for the drive/brake torque. This requires computation of the variance of the vector $\mathbf{u}_k$. In order to achieve this, $\mathbf{u}_k$ is split into nominal and perturbed components:

$$\text{cov}(\mathbf{u}_k) = \text{cov}(\bar{\mathbf{u}}_k + \Delta\mathbf{u}_k) = \text{cov}(\Delta\mathbf{u}_k) = \text{cov}(-\mathbf{K}_k\Delta\mathbf{x}_k) \tag{41}$$

Making again use of the identity $\text{cov}(\mathbf{Ab}) = \mathbf{A}\text{cov}(\mathbf{b})\mathbf{A}^T$, the following is obtained

$$\text{cov}(\Delta\mathbf{u}_k) = \mathbf{K}_k\text{cov}(\Delta\mathbf{x}_k)\mathbf{K}_k^T \tag{42}$$

Thus, once the state-covariance is computed at each time-step, the covariance matrix of the input vector can be found using (42). A comparison of the analytical and numerical results is shown in Fig. 9, which confirms the validity of the method.

6 Results

Fig. 10 shows the standard deviation of the lateral path error as the two vehicles travel around the corner. On approach to the bend the error is about 0.04 m but the error increases as the vehicles pass the apex of the bend, reaching a maximum between the apex and exit of the bend. The two vechicles behave similarly, although the OS vehicle experiences a higher maximum value of path error standard deviation, about 0.15 m. Comparison to the nominal control actions in Fig. 4 and Fig. 5 shows that the increase in path error begins some distance after the braking point, once the steering angle has reached about half its peak positive value. Once accelerating in a straightline after the exit of the bend the path error reduces to the about the value seen before braking on approach to the bend.

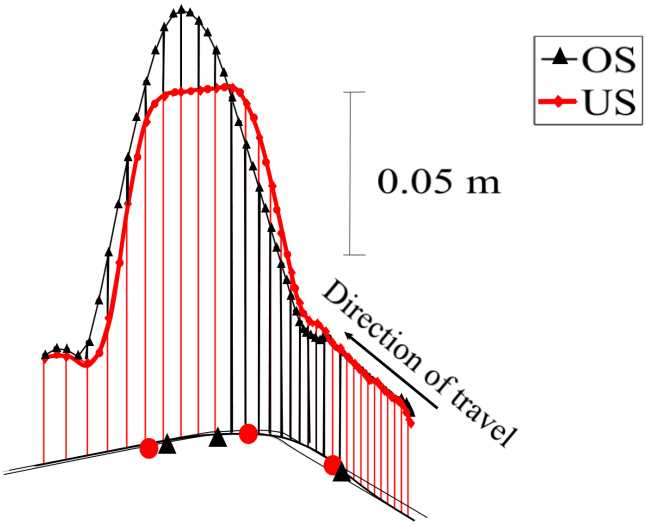

Fig. 10: Standard deviation of lateral path error through the manoeuvre.

Fig. 11 shows the corresponding results for the heading error. The trends are similar, although heading error begins increasing later in the manoeuvre than lateral error. The OS vehicle exhibits two peaks, which occur either side of the switch from braking to accelerating.

Fig. 12 shows the standard deviation of the compensatory hand wheel angle. The increase in lateral and heading error is generally matched by increase in the compensatory hand wheel angle. The US vehicle has two peaks, located each side of the switch from braking to accelerating. The OS vehicle has a large peak just before the switch from braking to accelerating, and coincident with the first peak in heading error shown in Fig. 11

Further insight to the effect of the centre of mass position can be gained by plotting the standard deviations as a function of time and of CoM position, however in this format it is more difficult to relate feaures of the surface plot to locations on the bend. Fig. 13 shows the standard deviation of the compensatory steering control. The US and OS vehicles correspond to the edges of the surface, at $a/(a+b) = 0.4$ and $a/(a+b) = 0.6$.

7 Discussion

In this section the response variances of the compensatory steering controller are compared to some of the existing stability criteria reviewed in Section 1, specifically stability and controllability derivatives, and frozen-time eigenvalues. These existing criteria are evaluated by considering only the linearised lateral-yaw dynamics of the vehicle (3a) and (3b) and linearising the combined slip tyre model at each point

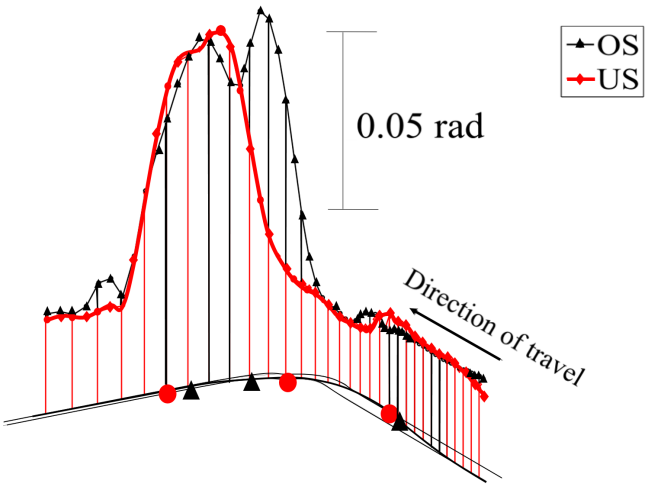

Fig. 11: Standard deviation of heading error through the manoeuvre.

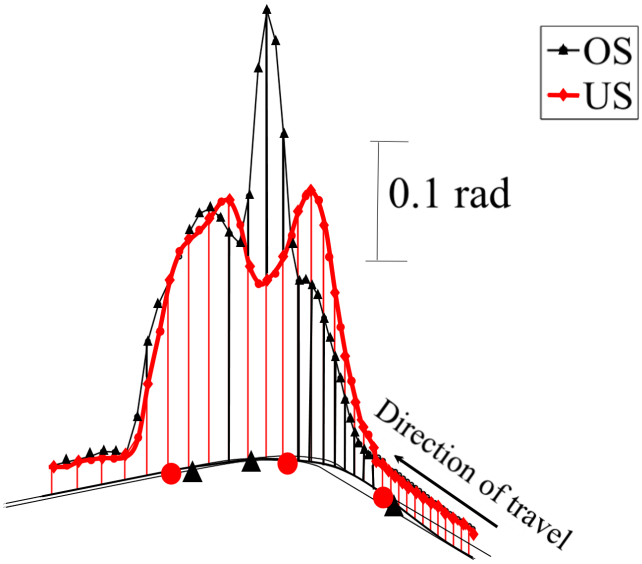

Fig. 12: Standard deviation of compensatory hand wheel angle through the manoeuvre.

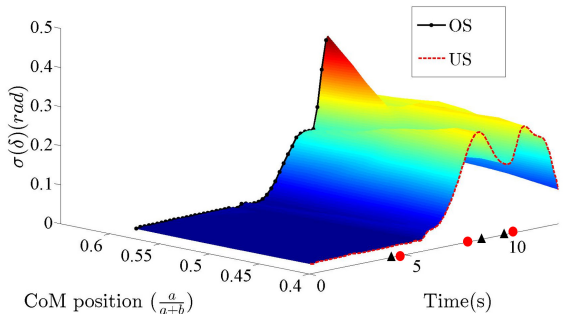

Fig. 13: Surface plot showing how the standard deviation of the compensatory hand wheel angle varies with CoM position and time through the manoeuvre. The US and OS vehicles correspond to the boundaries of the surface.

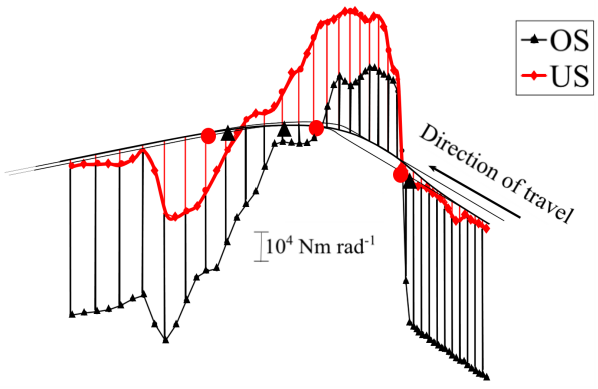

Fig. 14: Directional stablilty derivative for the OS and US vehicles through the manoeuvre.

through the manoeuvre.

Fig. 14 shows the variation of the directional stability derivative $\partial M_t/\partial\beta$ as the US and OS vehicles travel through the curve. On approach to the curve the derivative is negative, which indicates a destabilising condition and arises because the traction force at the rear wheels decreases the effective cornering stiffness at the rear axle. After the braking point the derivative becomes positive, consistent with the stabilising effect of the front-biased brake balance. The subsequent changes of sign in the derivatives approximately follows the switches between drive and brake torque shown in Fig. 4, consistent with the combined slip behaviour of the tyres. Comparison with the responses of the compensatory dynamics in Figs. 10 to 12 reveals that the standard deviation of the compensatory control actions does not correlate well with the directional stability derivative: the control actions are large in regions of positive and in regions of negative derivative.

Fig. 15 shows the variation of the yaw damping derivative $\partial M_t/\partial\psi$ as the vehicles travel through the curve. The US and OS vehicles exhibit a similar variation. The derivative is negative throughout the manoeuvre, corresponding to a stabilising action. However the derivative reduces signicantly in the middle of the manoeuvre, corresponding approximately to the peaks in the compensatory responses in Figs. 10 to 12. The derivative tends to increase with a reduction in vehicle speed, theoretically approach infinity as the speed approaches zero. The indicates that the decrease in effective cornering stiffness of the the tyres

Fig. 16 shows the variation of the control moment derivative $\partial M_t/\partial\delta_{sw}$ as the vehicles travel through the curve. The derivative is high whilst the vehicle is accelerating on approach to the curve because there are no drive or braking torques on the front axle to reduce the cornering stiffness. The derivative reduces significantly once the brakes are applied, and reduces further as hand wheel angle is applied and the front tyre nears saturation. The US vehicle reaches a significantly lower value than the OS vehicle because of the

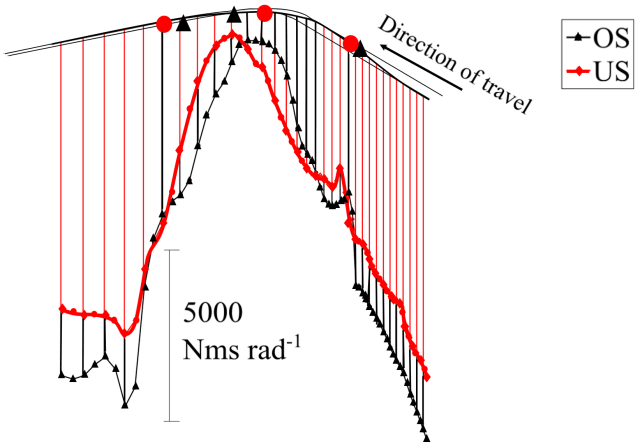

Fig. 15: Yaw damping derivative for the OS and US vehicles through the manoeuvre

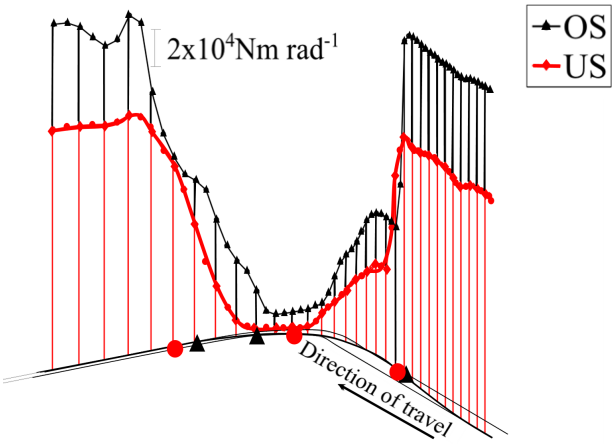

Fig. 16: Control moment derivative for the US and OS vehicles through the manoeuvre

forward CoM position of the US vehicle. The trough in the derivative corresponds approximately to the peak region of the compensatory hand wheel angle in Fig. 12.

Fig. 17 shows the real and imaginary parts of the eigenvalues for the lateral-yaw dynamics of the US vehicle through the manoeuvre. The circles plotted on the time axis correspond to the three phases of the manouvre: braking on entry; transition from braking to accelerating at mid corner; and maximum drive torque at exit. Positive real parts indicate instability; non-zero imaginary parts indicate oscillation. The vehicle is stable throughout the manoeuvre apart from the point where drive torque is applied at mid-corner until just after the point where maximum drive torque hs been applied at exit. Fig. 18 shows the eigenvalues for the OS vehicle. In comparison to the US vehicle, it becomes unstable earlier in the maoeuvre (mid-way through the braking phase) but returns to stability at about the same time. Comparing this data to the response variances of the compensatory control, Figs. 10 to 12 does not show an obvious relationship to the features of the variance data, apart from a general increase in

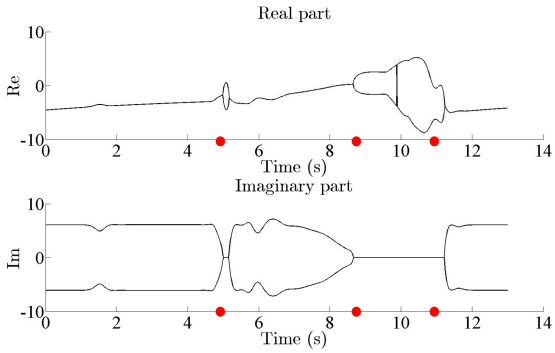

Fig. 17: Eigenvalues for the US vehicle going through the manoeuvre described in Section 3. The circles plotted on the time axis correspond to the three phases of the manouvre: braking on entry; transition from braking to accelerating at mid corner; and maximum drive torque at exit. Positive real parts indicate instability; non-zero imaginary parts indicate oscillation.

variance in the regions of instability.

It is clear from the comparisons made in this Section that the response variances of the driver and vehicle compensatory dynamics give an additional view of the behaviour of a nonlinear vehicle as it travels through a manoeuvre near to the limit of adhesion. Further work is needed to understand precisely how the responses should be interpreted, and to investigate the effect of the neuromuscular properties (damping and natural frequency). A series of instrumented vehicle or driving simulator experiments with experienced drivers providing subjective assessments is an obvious next step. It is anticipated that such experimental data will allow potential benefits of the new criteria to be revealed. Other extensions to the work are planned: addition of human sensory and cognitive limitations to the compensatory control model; a nonlinear instead of linear compensatory controller; and incorporation of the compensatory response variances as constraints in the calculation of the nominal optimal controls. An important step in all these developments will be experimental validation of the driver's feedforward and feedback control strategies and of the relationship between objective and subjective responses.

8 Conclusion

A brief review of existing criteria for quantifying stability and controllability of road vehicles concluded that the *practical stability* approach was worthy of further development, with the aim of providing a closer relationship to subjective assessments by drivers. A minimum manoeuvre time calculation for a five DoF nonlinear vehicle model revealed that moving the CoM rearwards (without changing the brake balance) required earlier braking on entry to the corner, countersteering between mid-corner and exit, and later acceleration out the corner. Calculation of the response variances of a

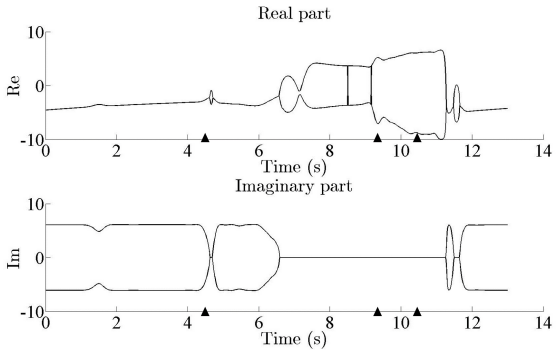

Fig. 18: Eigenvalues for the OS vehicle going through the manoeuvre described in Section 3.

compensatory LQR steering controller agreed closely with the variances calculated from an ensemble of time-domain responses, and thus enabled efficient computation of the driver and vehicle response to random distrubances acting on the vehicle as it travels through the manoeuvre. The variance of lateral path error, heading error and compensatory hand wheel angle plotted as a function of distance through the corner revealed how the driver might perceive the change in vehicle operating point. The main effect of moving the centre of mass rearwards was a sharp increase in the variance of the hand wheel angle at the transition from braking to accelerating at mid-corner. Comparison of the variances to existing criteria (eigenvalues and stability derivatives) demonstrated that the new criteria present an additional perspective of the dynamic behaviour of a nonlinear vehicle through the manoeuvre. Further work is planned, including comparison of the new stability and controllability criteria with subjective assessments by a human driver.

Acknowledgements

This work was partly supported by: the Engineering and Physical Sciences Research Council (studentships for Timings and Braghieri) (EP/P505445/1); and Lotus F1 Team (now Renault Sport F1 Team) (RG57218, RG72244). Supporting data are available at Cambridge University digital repository: https://www.repository.cam.ac.uk.

References

[1] Milliken, W., and Milliken, D., 1995. *Race car vehicle dynamics*. Society of Automotive Engineers, Warrendale, PA.

[2] Pacejka, H., 2002. *Tyre and vehicle dynamics*. Butterworth Heineman, Oxford.

[3] Ono, E., Hosoe, S., Tuan, H., and Doi, S., 1998. "Bifurcation in vehicle dynamics and robust front wheel steering control". *IEEE Transactions on Control Systems Technology,* **6**(3), May, pp. 412 – 420.

[4] Nguyen, V., 2005. "Vehicle handling, stability and bifurcation analysis for nonlinear vehicles models". Master's thesis, Univeristy of Maryland.

[5] Skoog, R., and Lau, C., 1972. "Instability of slowly varying systems". *IEEE Transactions on Automatic Control,* **17**(1), pp. 86–92.

[6] Desoer, C., 1969. "Slowly varying system xdot=a(t)x". *IEEE Transactions on Automatic Control,* **14**(6), Dec, pp. 780–781.

[7] Limebeer, D., Sharp, R., and Evangelou, S., 2001. "The stability of motorcycles under acceleration and braking". *Proceedings IMechE, Part C,* **215**, pp. 1095–1109.

[8] Meijaard, J., and Popov, A., 2008. "Practical stability analysis for transient system dynamics". *Proceedings of the Royal Society of London,* **463**(2084), pp. 2123–2135.

[9] Timings, J., and Cole, D., 2014. "Robust lap-time simulation". *Proceedings IMechE, Part D, Journal of Automobile Engineering,* **228**(10), September, pp. 1200–1216.

[10] Sideris, M., 2011. "F1 car stability analysis". Masters thesis, Cambridge University Engineering Department.

[11] Haslam, A., 2012. "Stability and controllability of a formula one racing car". Masters thesis, Cambridge University Engineering Department.

[12] Best, M., and Gordon, T., 2006. "On the synthesis of inputs for the simulation of closed-loop handling manoeuvres". *International Journal of Vehicle Design,* **40**(1/2/3), pp. 52–76.

[13] Odhams, A., and Cole, D., 2014. "Identification of preview steering control models using data from a driving simulator and a randomly curved road path". *International Journal of Autonomous Vehicle Systems,* **12**(1), pp. 44–64.

[14] Cole, D., Pick, A., and Odhams, A. M. C., 2006. "Predictive and linear quadratic methods for potential application to modelling driver steering control". *Vehicle System Dynamics,* **44**(3), pp. 259–284.

[15] Cole, D., and Pick, A., 2007. "Dynamic properties of a driver's arms holding a steering wheel". *Proceedings of the Institution of Mechanical Engineers, Part D,* **221**, pp. 1475–1486.

[16] Timings, J., and Cole, D., 2013. "Minimum manoeuvre time calculation using convex optimisation". *ASME Journal of Dynamic Systems, Measurement and Control,* **135**(031015), May.

[17] Ulsoy, A., Lin, C., and LeBlanc, D., 2000. "Vehicle dynamics and external disturbance estimation for vehicle path prediction". *Control Systems Technology, IEEE Transactions,* **8**(3), May, pp. 508–518.

[18] Keen, S., and Cole, D., 2012. "Bias-free identification of a linear model predictive steering controller from measured driver steering behavior". *IEEE Transactions on Systems, Man and Cybernetics, Part B,* **42**(2), pp. 434–443.

[19] Johns, T., and Cole, D., 2015. "Measurement and mathematical model of a driver's intermittent compensatory steering control". *Vehicle System Dynamics,* **53**(12), pp. 1811–1829.

[20] Nash, C., and Cole, D., 2015. "Development of a novel model of driver-vehicle steering control incorporating sensory dynamics". In Proceedings of IAVSD Symposium on Vehicles on Roads and Tracks, Graz, Austria.

[21] Dorf, R., 1980. *Modern Control Systems*. Addison-Wesley Series in Electrical Engineering. Addison-Wesley, Reading, Mass.

[22] Grewal, M., and Andrews, A., 2008. *Kalman Filtering: Theory and Practice Using MATLAB*. Wiley-IEEE Press, New York, NY.

[23] Apetaur, M., and Opicka, F., 1992. "Assessment of the driver's effort in typical driving manoeuvres for different vehicle configurations and managements". *International Journal of Vehicle Mechanics and Mobility,* **20**, pp. 42–56.